ACS OMEGA

Open Access

http://pubs.acs.org/journal/acsodf

Article

Capturing Acidic CO_2 Using Surface-Active Difunctional Core–Shell Composite Polymer Particles via an Aqueous Medium

M. Asheq Mahamud, A. S. M. Maruf Galib, Md. Muhyminul Islam, Md. Mahiuddin, Md. Abdur Rahman,* Md. Mahbubor Rahman, Md. Shahidul Islam, Hasan Ahmad, and Md. Ashraful Alam*

Cite This: *ACS Omega* 2023, 8, 44523–44536

Read Online

ACCESS | Metrics & More | Article Recommendations | Supporting Information

ABSTRACT: Multifunctional surface-active polymeric composites are attractive materials for the adsorption of various small molecules. Herein, dual-functionalized micron-sized surface-active composite polymer particles were prepared by a three-step process for CO_2 adsorption. First, polystyrene (PS) seed particles were prepared via the dispersion polymerization of styrene. PS/P(MMA-AAm-EGDMA) composite polymer particles were then synthesized by aqueous seeded copolymerization of methyl methacrylate (MMA) and acrylamide (AAm) in the presence of an ethylene glycol dimethacrylate (EGDMA) cross-linker. Finally, the amide moieties of PS/P(MMA-AAm-EGDMA) composite particles were converted into an amine-functionalized composite by using the Hofmann degradation reaction. The presence of primary amine groups on the surface of aminated composite particles was confirmed by some conventional chemical routes, such as diazotization and Schiff's base formation reactions. The formation and functionality of the PS seed, PS/P(MMA-AAm-EGDMA), and aminated PS/P(MMA-AAm-EGDMA) composite polymer particles were confirmed by Fourier transform infrared (FTIR) spectra analyses. Scanning electron microscopy (SEM) analysis revealed spherical shape, size, and surface morphologies of the PS seed, reference composite, and aminated composites. The elemental surface compositions, surface porosity, pore volume, pore diameter, and surface area of both composite particles were evaluated by energy-dispersive X-ray (EDX) mapping, X-ray photoelectron spectroscopy, and Brunauer–Emmett–Teller (BET) and Barrett–Joyner–Halenda (BJH) analyses. Dynamic light scattering (DLS) and ζ-potential measurements confirmed the pH-dependent surface properties of the functionalized particles. The amount of the adsorbed anionic emulsifier, sodium dodecyl sulfate (SDS), on the surface of aminated PS/P(MMA-AAm-EGDMA) is higher at pH 4 than that at pH 10. A vice versa result was found in the case of cationic surfactant, hexadecyltrimethylammonium bromide (HTABr), adsorption. Synthesized aminated composite particles were used as an adsorbent for CO_2 adsorption via bubbling CO_2 in an aqueous medium. The changes in dispersion pH were monitored continuously during the adsorption of CO_2 under various conditions. The amount of CO_2 adsorption by aminated composite particles was found to be 209 mg/g, which is almost double that of reference composite particles.

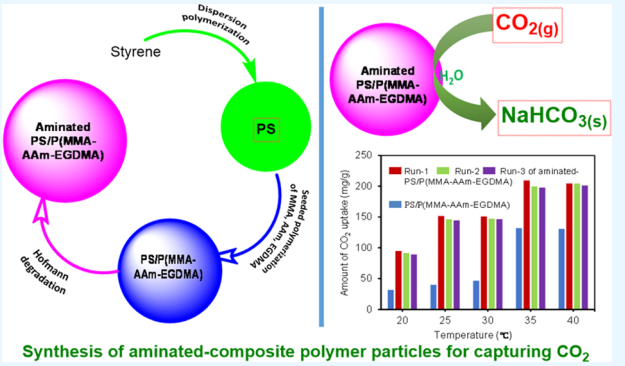

Synthesis of aminated-composite polymer particles for capturing CO_2

INTRODUCTION

Rising atmospheric temperature, melting glaciers, rising global sea levels, devastating floods, unbearable drought, etc., are the various signs of global warming. Global warming is caused by the emission of greenhouse gases, such as CO_2, CH_4, N_2O, hydrofluorocarbons (HFCs), perfluorocarbons (PFCs), SF_6, NF_3, and O_3. Among these, CO_2 has the highest contribution[1] to the greenhouse effect and is recognized as the world's number one problem after the industrial revolution. In this perspective, both the reduction of CO_2 emission and capture from point sources, such as fossil fuel-based power plants, and from the atmosphere are very important to save the environment from global warming.[2] In doing this, modern, sustainable, and environmentally friendly methods and materials are very essential.

Various methods, including liquid amine absorption, adsorption membrane separation[3−10] etc., have been suggested for CO_2 capture. More precisely, amine solvent-based CO_2 absorption is the most promising technique. In spite of having high adsorption efficiency, some disadvantages, including high

Received: April 30, 2023
Revised: October 5, 2023
Accepted: October 10, 2023
Published: November 14, 2023

Scheme 1. Preparation of the PS Seed, Transformation of PS Seeds into PS/P(MMA-AAm-EGDMA) Composite Particles, and Their Conversion to Amine-Functionalized PS/P(MMA-AAm-EGDMA) Composite Polymer Particles

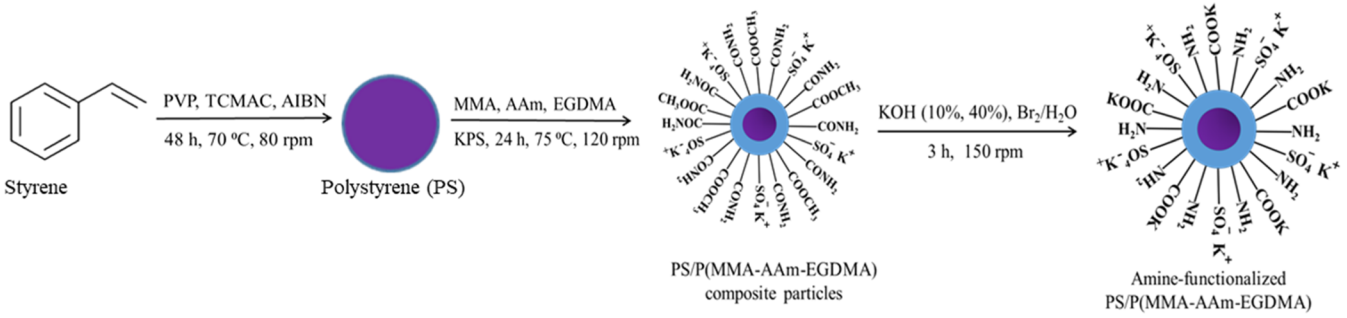

regeneration energy, especially designed large equipment requirements, solvent degradation, and equipment corrosion, have made it less feasible. To overcome such drawbacks, adsorptive separation is considered one of the alternative and attractive techniques because of low heat regeneration, higher adsorption capacity, and good adsorption kinetics.[11−16] Several conventional materials such as zeolites, carbonaceous materials, silica, chitosan (CS), and metal−organic frameworks (MOFs) have widely been investigated as adsorbents for adsorptive separation of CO_2.[3−9]

It is believed that high-density amine functionalization of adsorbents would improve the CO_2 adsorption capacity and selectivity in both the absence and presence of H_2O vapor, facilitating fast adsorption and desorption kinetics and easy recovery.[4−9,17−20] The present investigation is aimed at designing an amine-functionalized composite polymer for adsorbing CO_2 from aqueous solution. The composite polymers are generally known for their high flexural strength, tensile strength, impact strength, compressive strength, Young's modulus, lightweight, and rigidity along with high dimensional stability.[21] To the best of our knowledge, no work is available on the application of amine-functionalized polymers for CO_2 absorption. However, some literature describes the preparation and applications of amine-functionalized conventional adsorbents. For example, Drese et al. studied the synthesis of hyperbranched amino silica for CO_2 adsorption. This functional silica displayed a considerably high CO_2 adsorption capacity ranging from 2.0 to 5.6 mmol/g.[22] Qi et al. synthesized amine-functionalized mesoporous silica capsules impregnated with polyethylenimine (PEI) and tetraethylenepentamine (TEPA) and achieved high CO_2 adsorption efficiency in the range of 4.5−7.9 mmol/g.[23] Dao et al. also modified silica materials having different pore volumes with various amines and achieved adsorption capacity as high as 5.91 mmol/g.[24] PEI-functionalized porous chitosan (PEI-CS) beads are also applied for CO_2 capture in the absence and presence of water vapor.[25,26] Regarding polymeric materials, it is worth mentioning that some researchers described the usefulness of hypercross-linked porous organic polymers for CO_2 capture.[27−30] These porous polymers obviously possessed higher adsorption capacity, but they required a tedious synthesis route and sometimes possessed an inaccessible binding site that resulted in poor binding efficiency.

Herein, polystyrene/poly(methyl methacrylate-*co*-acrylamide-ethylene glycol methacrylate) composite polymer particles named PS/P(MMA-AAm-EGDMA) were first prepared. The PS core is used to introduce some sort of rigidity to the adsorbent, and the PMMA component functions as a filler and a hydrophobicizing agent for the water-soluble PAAm segment in the copolymer. The Hofmann degradation reaction[31] of PS/P(MMA-AAm-EGDMA) composite polymer particles is then carried out to introduce the primary amine ($-NH_2$) group on the particle surface. During such a degradation reaction, carboxylate groups can also be generated from the hydrolysis of ester, producing dual-responsive zwitterionic composite polymer particles. The potentiality of prepared composite polymer particles is then tested for CO_2 adsorption. The adsorption efficiency was followed by monitoring the continuous pH change of the aqueous medium by using the $pH = -\log[H^+]$ relationship. CO_2 is an acidic gas. Interaction of water with CO_2 bubbling through aqueous dispersion containing an amine-functionalized composite polymer should lower the pH value of the acid−water medium through the generation of protons (H^+) and bicarbonate ions (HCO_3^-, Arrhenius concept).[32] Here, it is assumed that under the conditions, protonation of $-NH_2$ groups present on the particle surface would result in an increase in the pH of the aqueous system and subsequent hydrogen bonding and electrostatic adsorption of HCO_3^- ions. In this case, the protonation capacity and hence the adsorption of CO_2 passing through aqueous dispersion would be directly related to the density of amine functionality in the composite.

MATERIALS AND METHODS

Chemicals. Styrene purchased from Fluka, Chemika, Switzerland, was purified by washing with a 20% NaOH solution followed by distilled deionized water and finally passed through an activated basic alumina column before being preserved in a refrigerator. Both poly(vinylpyrrolidone) (PVP) and tricaprylylmethylammonium chloride (TCMAC) were bought from Fluka, Chemika, Switzerland. Azobis-(isobutyronitrile) (AIBN) was purchased from LOBA Chem, India. It was recrystallized from ethanol before use. Methyl methacrylate (MMA) of monomer grade, purchased from Fluka, Chemika, Switzerland, was purified by the chromatographic method, and acrylamide (AAm), bought from LOBA Chem., India, was recrystallized from water. Ethylene glycol dimethacrylate (EGDMA) purchased from Fluka, Chemika, Switzerland, a cross-linking agent, was used without any purification. Potassium persulfate (KPS) obtained from LOBA Chem., India, was recrystallized from distilled water before use. Sodium dodecyl sulfate (SDS) was purchased from Merck, Germany, and hexadecyltrimethylammonium bromide was purchased from Sigma-Aldrich. KOH pellet and bromine were of reagent grade. Benzaldehyde used for the formation of

https://doi.org/10.1021/acsomega.3c02976
ACS Omega 2023, 8, 44523−44536

Scheme 2. Preparation of the Diazonium Salt and Schiff's Base Product from Amine-Functionalized PS/P(MMA-AAm-EGDMA) Composite Polymer Particles

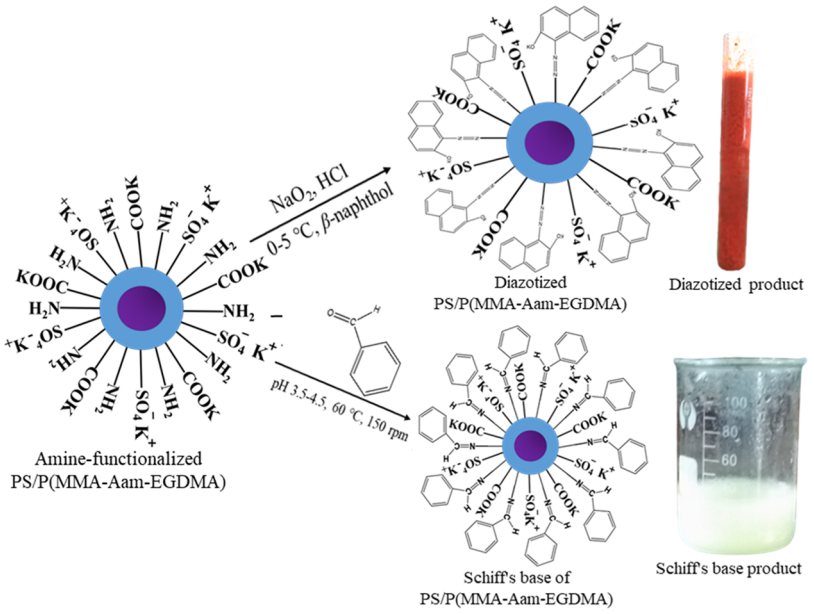

Schiff's base was purchased from Matheson−Coleman−Bell (MCB) Chemical Company. CO_2 used for adsorption was purchased from Qingdao Guida Special Gas Company Ltd., China. Other chemicals used were of reagent grade.

Preparation of Amine-Functionalized Composite Polymer Particles. Amine-functionalized PS/P(MMA-AAm-EGDMA) composite polymer particles were prepared by a simple three-step, which is shown in Scheme 1. First, micron-sized PS seed particles were synthesized by dispersion polymerization in a 250 mL three-necked round flask equipped with a reflux condenser and a mechanical stirrer. 17.0245 g of styrene was taken in the flask. The stabilizer mixture, prepared by mixing 0.6808 g of PVP and 0.1979 g of TCMAC in 70 mL of ethanol, was added into the reaction flask dipped in a thermostat water bath. The temperature was increased to 70 °C, and polymerization was started after adding 0.2567 g of the initiator (AIBN) dissolved in 20.0 mL of ethanol. The reaction was carried out for 24 h under a nitrogen atmosphere at a stirring speed of 80−82 rpm. The conversion of styrene to PS, measured gravimetrically, was 98.7% (Figure S1). In the second step, PS/P(MMA-AAm-EGDMA) composite polymer particles were prepared by maintaining a constant core−shell ratio of 1:0.44 via dropwise addition of a comonomer mixture (0.9890 g, 11.5 mmol of methyl methacrylate, MMA, 2.9548 g, 41.6 mmol of AAm and 0.2674 g, 1.6 mmol of ethylene glycol methacrylate, EGDMA) into the PS seed emulsion of 131.15 g (solid content 5.34 g%), using 0.0881g of kalium persulfate, KPS, as a water-soluble initiator. Tween 80 was used as an emulsifier, and water (35.5 g) was used as a solvent. The whole reaction was performed under a nitrogen gas atmosphere at 75 °C, 120 rpm in a three-necked flask equipped with a reflux condenser and a mechanical stirrer immersed in a water bath for 24 h. With the help of a centrifuge machine, the supernatant was discarded from the particles by washing them five times with distilled deionized water. The particles were dried by using a vacuum desiccator and preserved for further use. Finally, amino ($-NH_2$) groups were introduced to PS/P(MMA-AAm-EGDMA) composite polymer particles by Hofmann degradation of simple amide moieties of composite particles. In brief, 2.0 g of vacuum-dried PS/P(MMA-AAm-EGDMA) composite particles were taken in a 250 mL conical flask, 8 mL of bromine (1%) water was added into the flask, and stirring was started magnetically. A 10% KOH solution was first added dropwise by a buret until the brown color of the solution turned yellow, and then 50 mL of a 40% KOH solution was added at a time. The reaction was continued for 3 h with magnetic stirring at 150 rpm.

Instruments. Scanning electron microscopy (SEM, JSM-6510, JEOL, Tokyo, Japan) operated at 20 kV was used to check the surface morphology and size distribution of the prepared particles. The samples were diluted and dropped onto a mica sheet before being dried in a vacuum dryer. The dried particles were gold-coated before recording the SEM images. Elemental EDX mapping was performed using the aforementioned instrument. The change in surface functionality following modification of the PS particles was evaluated by FTIR spectroscopy (PerkinElmer, FTIR-100, Waltham, MA) over the range of 4000−200 cm^{-1} in KBr pellets. Elemental compositions were assessed by XPS equipped with monochromatic Al Kα radiation (1486.6 eV) at 20 kV, 104 W, and the X-ray current was 20 mA. The measurement chamber pressure was about 8.0×10^{-7} Pa. The step size was 0.25 eV and the passing energy was 280 eV for survey and narrow-scan spectra, respectively, using an XPS instrument (ESCA-3400, Shimadzu, Kyoto, Japan). The specific surface area (SBET) of the dried composites was determined using a nitrogen adsorption isotherm at a relative pressure of 0.0−0.5 at 77 K on a Quantachrome NOVA3000e instrument. The BJH method was used to measure the average pore diameter and pore volume from the resorptive segment of the isotherm. The samples were purged under ambient conditions for 3 h before analysis. Intensity-weighted average hydrodynamic diameters of the seed, reference composite, and amine-functionalized composite polymer particles were recorded by the dynamic laser scattering (DLS) method using a NICOMP 380 particle sizer (Santa Barbara, CA). A ζ-potential and particle size

https://doi.org/10.1021/acsomega.3c02976
ACS Omega 2023, 8, 44523−44536

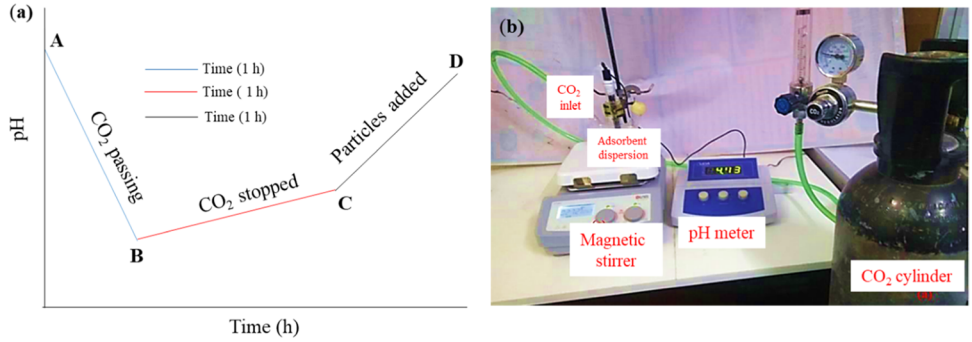

Figure 1. (a) Schematic representation for capturing CO_2 by amine-functionalized PS/P(MMA-AAm-EGDMA) and reference PS/P(MMA-AAm-EGDMA) composites. (b) Digital image of a typical instrumental setup used for CO_2 capturing.

analyzer (Zetasizer NanoZS, Malvern Instruments Limited, U.K.) was used for measuring the pH-dependent changes in the ζ-potential. A centrifuge machine (Kokuson Corporation Tokyo, Japan), a pH meter (MP220, Mettler Toledo, Switzerland), and a hot plate magnetic stirrer (DLAB, from China) were used in this study.

Measurement of the Hydrodynamic Diameter. By a dynamic laser scattering particle analyzer, the average diameters of the PS seed, PS/P(MMA-AAm-EGDMA), and aminated PS/P(MMA-AAm-EGDMA) composite polymer particles were measured at different pHs. Respective dispersion was diluted to around 0.1% solid using distilled deionized water before performing the measurement. Each measurement was done twice, and the average values were reported. The error in the average measurement was less than ±5%.

Confirmation of Amine Functionality in the Surface PS/P(MMA-AAm-EGDMA) Composite Polymer via Conventional Tests, Like Diazotization and Schiff's Base Formation Reactions. First, aminated PS/P(MMA-AAm-EGDMA) composite polymer particles were transformed into a diazonium salt (Scheme 2). In brief, a small amount of amine-functionalized composite polymer particles and a few mL of aqueous $NaNO_2$ and HCl were taken in a test tube, and then, the tube was placed in an ice-cold water bath. Then, alkaline 2-naphthol was taken in another test tube, which was poured into the diazotized polymeric sample. The mixture was allowed to relax in an ice-cold water bath for several minutes. An orange-red color appeared. The obtained product is shown in a test tube in Scheme 2. Then, aminated PS/P(MMA-AAm-EGDMA) composite polymer particles were converted into a Schiff's base (Scheme 2). Briefly, 0.50 g of amine-functionalized PS/P(MMA-AAm-EGDMA) composite polymer particles were taken in a 100 mL conical flask and acidified with aqueous HCl (pH 3.5−4.5). Benzaldehyde (1.50 g) was added to that conical flask, and the reaction was continued with magnetic stirring (150 rpm) for 30 min at 60 °C. The appearance of a white color product confirmed the formation of Schiff's base. A digital photograph of the washed Schiff's base product is shown on the right side of Scheme 2.

pH-Dependent Adsorption of Surfactants on PS/P(MMA-AAm-EGDMA) and Amine-Functionalized PS/P(MMA-AAm-EGDMA) Composite Polymer Particles. The magnitude of adsorption of an anionic emulsifier, SDS, and a cationic emulsifier, HTABr, onto reference PS/P(MMA-AAm-EGDMA) and aminated PS/P(MMA-AAm-EGDMA) composite polymer particles was measured at two different pH values of 2 and 10. In the case of each PS/P(MMA-AAm-EGDMA) and aminated PS/P(MMA-AAm-EGDMA) composite polymer particles, a suspension was produced by adding 0.025 g of composite polymer particles in a 100 mL beaker containing 25 mL of distilled deionized water. The pH values were immediately adjusted to 4 and 10 by either dilute HCl or KOH aqueous solution, respectively, and the conductance of the solution was measured. Then, the emulsifier was added to water and stirred at a stirring rate of 150 rpm for 2 h. In each case, the concentration of the emulsifier in the mixture was kept below the critical micelle concentration. In order to examine the adsorption behavior of the emulsifiers onto the composite polymer particles, the conductance was measured at 25 °C. The magnitude of the emulsifier adsorbed was calculated using calibration curves (Figures S3 and S4) for the emulsifier aqueous solution at pH values of 2 and 10.

Temperature-Dependent Capturing of CO_2 Gas by Amine-Functionalized PS/P(MMA-AAm-EGDMA) Composite Polymer Particles. The effectiveness of both reference PS/P(MMA-AAm-EGDMA) and amine-functionalized PS/P(MMA-AAm-EGDMA) composites for capturing CO_2 gas was tested by simple CO_2 bubbling in aqueous medium at different temperatures (20 to 45 °C). In detail, 100 mL of distilled deionized water was taken in a round-bottom three-necked flask equipped with a thermostat water bath and a magnetic heating stirrer. The pH value was recorded, which is indicated by point A in Figure 1a. Then, CO_2 gas was passed through the gas inlet in water for 1 h with magnetic stirring at 150 rpm. As a result, a gas−water mixture was produced, and the pH reached the lowest value at point B (Figure 1a). Then, the bubbling of CO_2 was stopped, but the mixture was continuously stirred for 1 h at 150 rpm to remove the excess CO_2 (free escaping) until the pH reached constant point C (Figure 1a). After reaching point C, a specific/variable amount of respective dried adsorbent particles was added to the flask, and stirring was continued for another 1 h. Therefore, the pH value of the dispersion mixture reached the highest value at point D in Figure 1a. The simple instrumental setup required for capturing CO_2 is shown in Figure 1b. The changes in pH values from point A to point D due to the presence and absence of CO_2, reference composite, and aminated composite particles are shown in Figure S1a,b. The amount of adsorbed CO_2 by composite particles was calculated by considering the difference in hydrogen ion concentration between point C and point D, using eq 1. The same procedure is maintained at different temperatures for capturing CO_2.

$$pH = -\log[H^+] \quad (1)$$

https://doi.org/10.1021/acsomega.3c02976
ACS Omega 2023, 8, 44523−44536

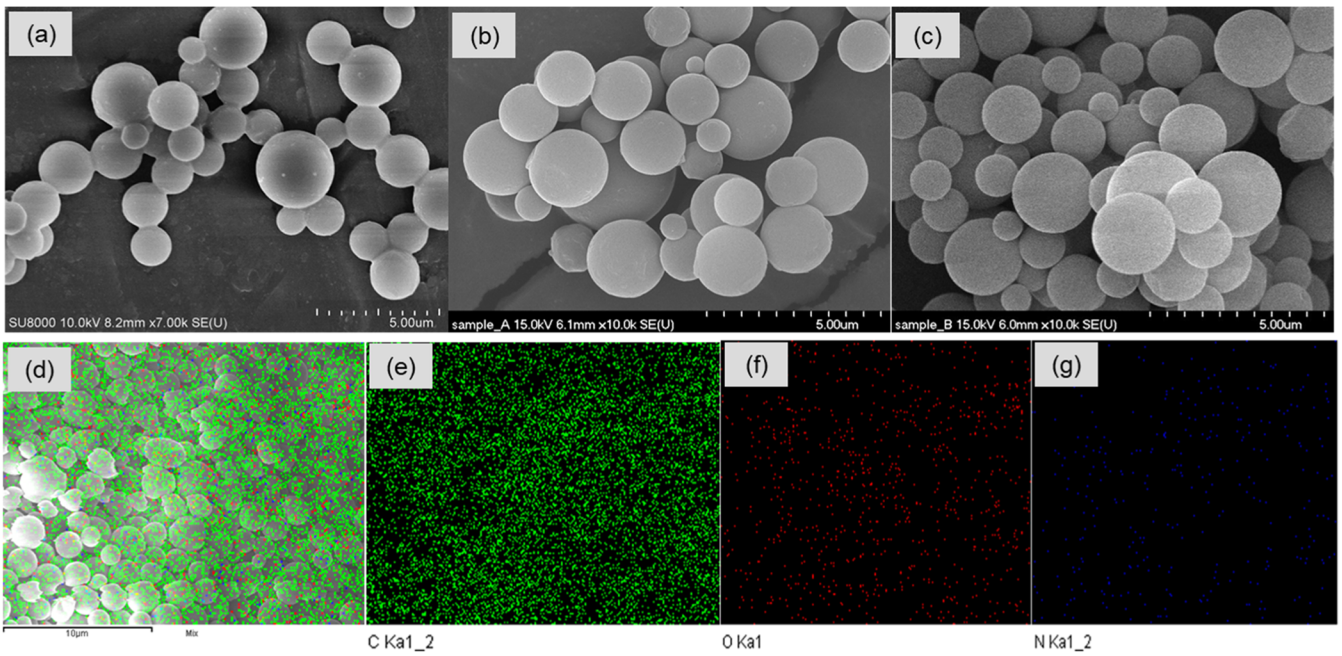

Figure 2. SEM images of PS seed (a); reference PS/P(MMA-AAm-EGDMA) (b); and aminated composite polymer particles (c). (d) SEM-EDX combined elemental mapping; and individual elemental mapping of carbon (e); oxygen (f); and nitrogen (g) of aminated PS/P(MMA-AAm-EGDMA) composite polymer particles.

Recovery and Reuse of CO_2-Adsorbed Amine-Functionalized PS/P(MMA-AAm-EGDMA) Composite Polymer Particles. To assess the recycling and reuse potentials of CO_2-adsorbed composite polymer particles, the gas-adsorbed particles were separated by centrifugation and dried in an electric oven for 1 h at 60 °C. Then, the dried particles were treated with 0.01 M NaOH for the removal of adsorbed CO_2 as $NaHCO_{3(s)}$. The free adsorbent particles were washed with distilled deionized water and reused for capturing CO_2up to three cycles.

RESULTS AND DISCUSSION

The amine-functionalized composite polymer particles were synthesized, characterized by using various techniques, and applied for acidic CO_2 capturing. To synthesize amine-functionalized particles, first, PS seed particles were prepared by the dispersion polymerization technique. The conversion of styrene into PS reached 100% within 24 h (Figure S2). The seeded emulsion copolymerization of MMA and AAm in the presence of the PS seed and a cross-linker, EGDMA, resulted in PS/P(MMA-AAm-EGDMA) composite particles. These composite particles were converted into amine-functionalized composite particles via simple Hofmann degradation of amide groups. The obtained aminated solid product is shown in Figure S3. The presence of amine moieties on the surface of composite particles was confirmed by chemical spectroscopic methods. The successful formation of the diazonium salt and Schiff's base product of the aminated composite confirmed the amination of the reference composite. The surface morphology, functionality, area, porosity, charge characteristics, and surface activity for capturing CO_2, recycling, and reusability of aminated composite polymer particles are discussed below.

The SEM images of the PS seed, reference PS/P(MMA-AAm-EGDMA), and amine-functionalized PS/P(MMA-AAm-EGDMA) composite polymer particles are shown in Figure 2a−c, respectively. The PS seed particles are spherical shaped with a smooth and hard surface, which is clearly visible in the SEM image. After seeded copolymerization of PS seed particles, the size increased and the surface morphology was also slightly improved.[33,34] However, successive amine functionalization of PS/P(MMA-AAm-EGDMA) particles fairly altered the surface topology, while the shape of the aminated composite particles was unchanged.[35] The average diameters of the PS seed (Figure 2a), reference composite (Figure 2b), and aminated composite polymer particles (Figure 2c) were 1706.61, 1976.56, and 1968.94 nm, respectively. The steady increase in average size indicates surface modification of PS seed particles with a copolymer shell. The copolymer shell thickness of the reference composite was measured to be around 269.95 nm. The amine-functionalized composite particle is smaller by 7.62 nm than the reference composite particles. This size depletion is most probable due to the hydrolysis of esteric groups and elimination of > CO moieties from $-CONH_2$ groups during the Hofmann degradation reaction. Although high polydispersity obviously affected the real measurement, the average hydrodynamic diameter measured by the NICOM particle sizer also showed an increasing trend, as noticed from the SEM images. The average hydrodynamic diameters for the PS seed, reference composite, and amine-functionalized composite polymers were 2054.3, 2144.6, and 4459.5 nm, respectively. The large increase in hydrodynamic diameter for amine-functionalized composite polymer particles is due to the insertion of more hydrophilic amine and carboxylic moieties as well as slight coagulation during alkali treatment during Hofmann degradation.[36] For all three particles, their average hydrodynamic diameter was slightly larger than the average diameters obtained from the SEM analyses. This increment in sizes is because of the hydration layers of polar groups via hydrogen bonding with water, while the SEM analyses were performed in the dried state of solid particles, where was not any possibility of swelling of the particles.[37,38] To evaluate

https://doi.org/10.1021/acsomega.3c02976
ACS Omega 2023, 8, 44523−44536

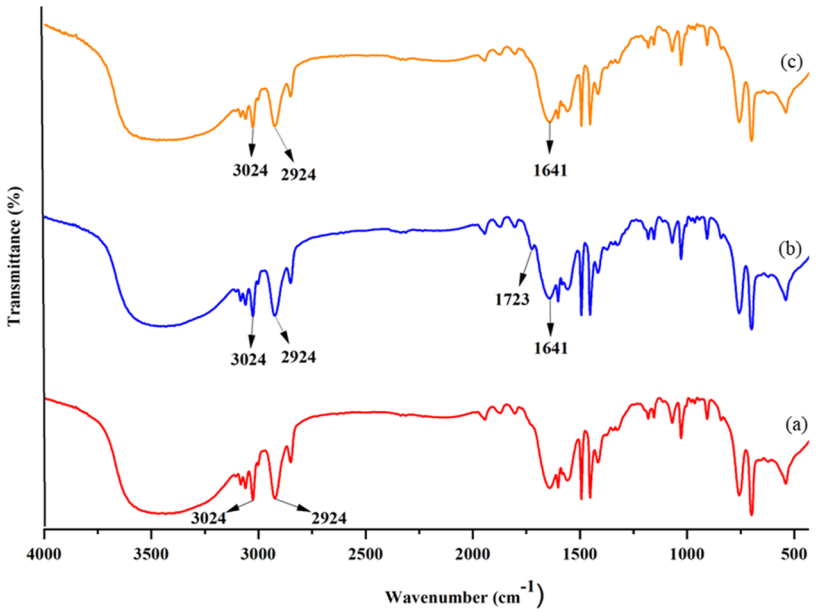

Figure 3. Compiled FTIR spectra of PS seed particles (a), reference PS/P(MMA-AAm-EGDMA) composite (b), and amine-functionalized PS/P(MMA-AAm-EGDMA) composite polymer particles (c).

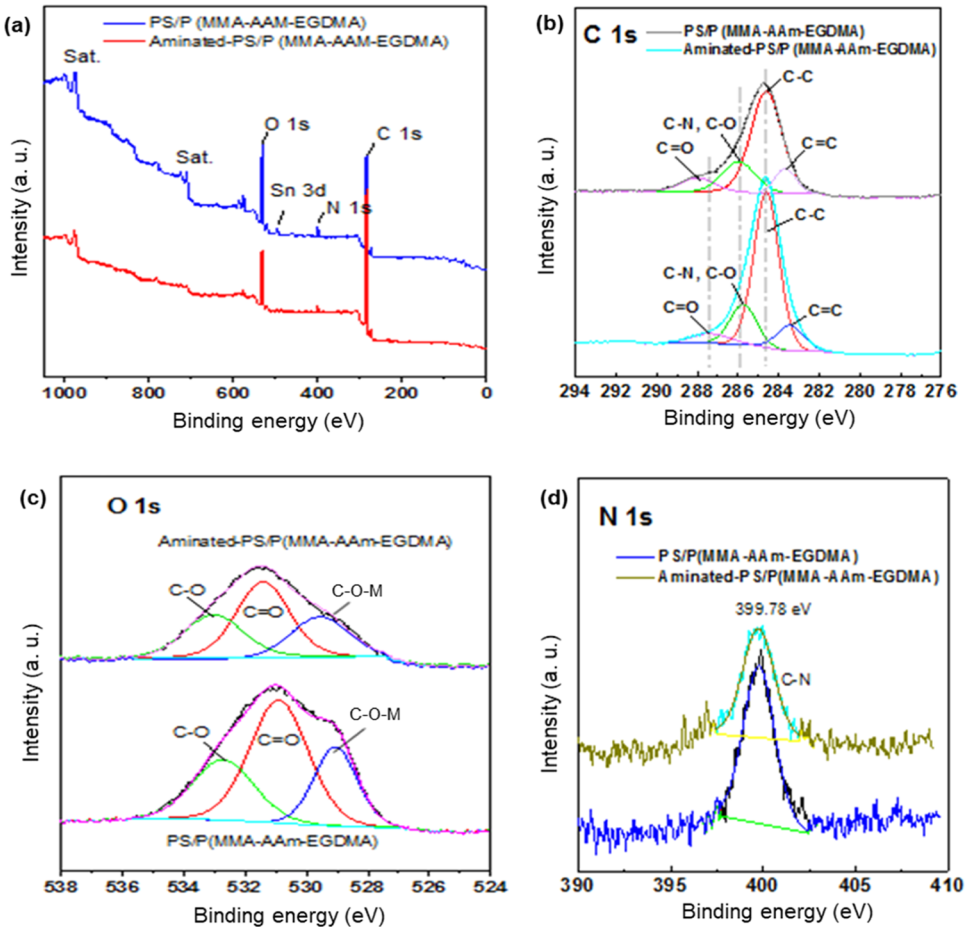

Figure 4. Compiled wide-scan survey XPS spectra (a) and narrow-scan (b) C 1s, (c) O 1s, and (d) N 1s core-line XPS spectra of reference PS/P(MMA-AAm-EGDMA) composite and amine-functionalized PS/P(MMA-AAm-EGDMA) composite polymer particles.

elemental compositions of the surface of both reference PS/P(MMA-AAm-EGDMA) and aminated PS/P(MMA-AAm-EGDMA) composite particles, SEM-EDX elemental mapping measurements were conducted, and the obtained data are shown in Figures S4and 2d−g, respectively. EDX elemental combined mapping revealed the presence of C, N, and O as

https://doi.org/10.1021/acsomega.3c02976
ACS Omega 2023, 8, 44523−44536

their elements in both the reference and aminated composites.[35] The individual atom distributions for C, N, and O were revealed from the surface of particles (Figure 2e−g).

Figure 3 shows the compiled FTIR spectra of PS seed particles (a), PS/P(MMA-AAm-EGDMA) composite (b), and amine-functionalized PS/P(MMA-AAm-EGDMA) composite polymer particles (c). Functional groups in the 4000−1500 cm^{-1} region showed different characteristic peaks for PS.[38−43] In the spectrum of PS seed particles, aliphatic and aromatic C−H stretching vibrations appeared at 2924 and 3024 cm^{-1}, respectively.[38,40] Aromatic C═C stretching vibrations of the phenyl group present as a pendent from the main chain appeared at 1446 and 1494 cm^{-1}.[38−40] No peak for the absorption of the C═C bond was found at 1630−1650 cm^{-1}. In the case of PS/P(MMA-AAm-EGDMA) composite polymer particles, the characteristic stretching bands of C−O−C and C═O were observed at 1341 and 1723 cm^{-1}, respectively, confirming the presence of ester[43,44] (Figure 3b). The characteristic stretching bands of C═O, N−H, and C−NH_2 due to amide groups appeared at 1667, 3196, and 3352 cm^{-1}, respectively.[45] Both PS seed and PS/P(MMA-AAm-EGDMA) composite polymer particles contained a broad O−H stretching band derived from adsorbed water. These results support the notion that the seeded copolymerization of MMA and AAm onto the surface of PS seed particles proceeded successfully. The FTIR spectrum of amine-functionalized PS/P(MMA-AAm-EGDMA) composite polymer particles exhibited a strong stretching band at 1641 cm^{-1}, which is assignable to the potassium salt of carboxylic acid (Figure 3c). The bands at 1619 and 3409 cm^{-1} refer to the NH_2 bending of the free NH_2 group and N−H stretching vibrations, respectively.[46,47] The appearance of the stretching band of −COOK and −NH_2 groups and, at the same time, the absence of the stretching band of ester and amide groups in the amine-functionalized PS/P(MMA-AAm-EGDMA) composite polymer particles proved that the Hoffmann degradation converted the amide and ester groups into primary amine and −COOK groups by basic hydrolysis.[48−50]

The surface compositions of both the reference and aminated composites were further studied by analyzing X-ray photoelectron spectroscopic (XPS) data. The XPS wide-scan survey spectra of the composites are shown in Figure 4a. Both the XPS spectra of reference PS/P(MMA-AAm-EGDMA) composite and amine-functionalized PS/P(MMA-AAm-EGDMA) composite polymer particles showed some peaks at the respective binding energy regions, i.e., 280−289, 524−536, and 396−402 eV, which are assignable to the C-, N-, and O-containing bonds as their building elements, respectively.[51−53] However, an additional minor peak related to the residual 3d Sn appeared in the XPS spectrum of the aminated composite. The surface compositions were assessed by atom %, which are shown in Table 1 for both reference and aminated composites. Both C and O atom % increased compared to the reference composite. However, N atom % decreased due to the basic hydrolytic cleavage of amide groups.

Table 1. Elemental Compositions of the Surface of Both Composites Determined by XPS Spectra Analysis

	calculated elemental composition from XPS spectra (atom %)		
polymer composite	carbon	oxygen	nitrogen
reference PS/P(MMA-AAm-EGDMA)	67.65	29.51	2.84
aminated PS/P(MMA-AAm-EGDMA)	79.76	18.25	1.99

The structure and functionality aspects regarding present elements and their oxidation states were also analyzed by studying the narrow-scan XPS spectra.[52−54] For the aminated composite particle surface, the presence of elemental functionality was investigated using C 1s, N 1s, and O 1s narrow-scan spectra, and the data were compared with the reference composite, which is shown in Figure 4b−d. In the narrow-scan C 1s spectrum (Figure 4b) of the aminated composite, a slightly shifted broadband appeared at 290.64−279.58 eV, which was deconvoluted to show the presence of different bonding patterns of carbon atoms with other elements in the composites. In the deconvoluted data, some broadbands appeared at 281−284, 282−287, 284−286, and 283−290 eV, which are assigned to the characteristic bands for C═C, C−C, C−O, and C−N and C═O bonds, respectively.[54−56] The peak intensities for the C═C, C−C, and C−O bands increased, although the C═O band was quite flattened compared to the reference composite. In a similar manner to C 1s, the narrow-scan O 1s spectrum (Figure 4c) also showed a broad signal at 536.5−525.52 eV for oxygen-related bonds with other elements, like C, N, etc. After deconvolution of the data, a series of fairly broadbands were observable at 526−532, 527−534, and 530−536 eV. These bands are assignable to the significant binding energy of O−M, C═O, and C−O bonds, respectively.[55,56] All these band intensities of the aminated composite were less flattened than the reference composite. Lastly, in Figure 4d, the narrow-scan N 1s spectrum of the aminated composite was compared with that of the reference composite. A broadband appeared at 403−397 eV for the C−N bond. The C−N band intensity slightly decreased compared to the reference composite due to the basic hydrolytic conversion of amide into carboxylate moieties.[49,50] The appearance of all these peaks and their respective intensity changes in XPS data validate the results that were demonstrated from the SEM, SEM-EDX, and FTIR, and successful surface modification of PS seed particles with the copolymer and their amine functionalization via the Hofmann degradation reaction.

Figure 5 shows the variation of average hydrodynamic diameters with changing pH values. The average diameter of PS seed particles (Figure 5a) remained constant with changing pH values because of the functionally inert and hydrophobic nature of the surface. In the case of PS/P(MMA-AAm-EGDMA) composite polymer particles (Figure 5b), the average hydrodynamic diameter increased slowly with increasing pH value from 2 to 6 and then remained almost constant up to pH 10. At pH 2, the average hydrodynamic diameter was 2144.6 nm, which increased to 2255.7 nm at pH 6. The partial hydrolysis of esteric groups and degradation of amide groups at lower pH plausibly accounted for the improvement in the stability of the colloidal suspension.[49,50] At pH 6, such reactions are nullified. Comparatively, in the case of amine-functionalized PS/P(MMA-AAm-EGDMA) composite polymer particles, a sharp descending trend in the average hydrodynamic diameter occurred from pH 2 to 4. At pH 2, the higher hydrodynamic diameter resulted from large swelling due to the protonation of −NH_2 groups into −NH_3^+, and −COOH groups were converted into −$COOH_2^+$. The minimum hydrodynamic diameter was noticed in the pH range of 4−6. Therefore, no swelling was observed for the amine

https://doi.org/10.1021/acsomega.3c02976
ACS Omega 2023, 8, 44523−44536

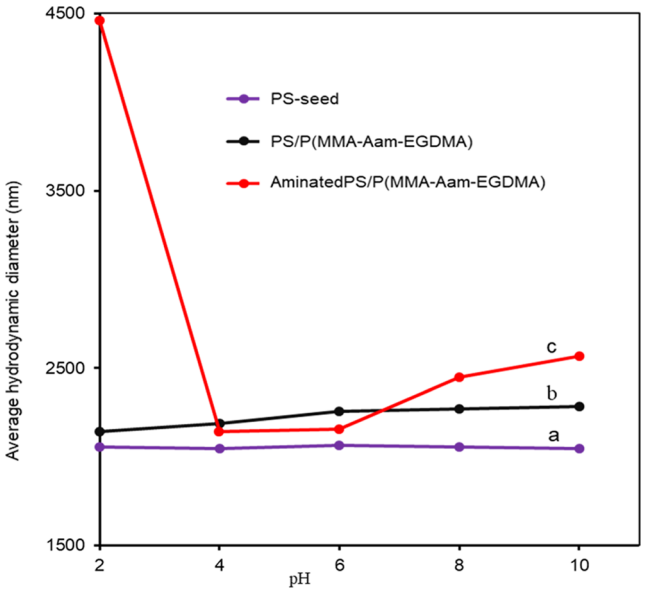

Figure 5. pH-dependent average hydrodynamic diameter of PS seed particles (a), reference PS/P(MMA-AAm-EGDMA) composite (b), and amine-functionalized PS/P(MMA-AAm-EGDMA) composite polymer particles (c) measured at 25 °C.

functional composite polymer particles in this range of pH. By further increasing the pH value to 10, a steady increase was observed in the hydrodynamic diameter, as −COOH groups were deprotonated to $-COO^-$ ions (Figure 5c).

Figure 6 represents the particle surface charge variations with changing dispersion pH values measured at 25 °C. A very

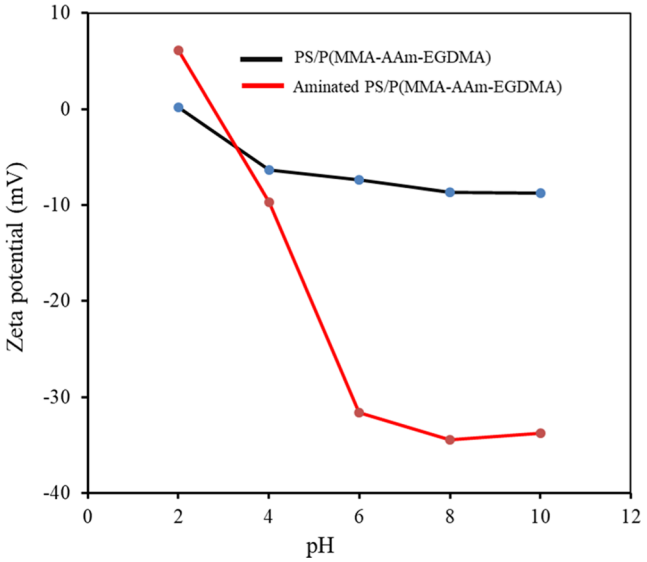

Figure 6. pH-dependent surface charge variation of amine-functionalized PS/P(MMA-AAm-EGDMA) and reference PS/P(MMA-AAm-EGDMA) composite polymer particles measured at 25 °C in an aqueous medium.

small quantity of positive charge (+0.21 mV) is developed for the reference PS/P(MMA-AAm-EGDMA) composite particles at pH 2. It is due to the protonation of intermediate amide groups present on the particle surface[57] and neutralization of the negative surface sulfate group derived from polymerizing persulfate initiator fragments. When the pH was increased from 2 to 4, the surface negative charge (−6.36 mV at pH 4) was developed, and the surface negative charge density remained almost steady in the pH range of 8−10. It is to be mentioned that prepared composite particles are negatively charged under the studied pH due to the presence of negative sulfate groups. Interestingly, the amine-functionalized PS/P(MMA-AAm-EGDMA) composite polymer showed a remarkably higher amount of positive surface charge (+6.11 mV) at pH 2. This positive charge is due to the protonation of amine and −COOH groups present on the particles' surface. When the pH was increased from 2 to 4, the negative charge (−9.74 mV at pH 4) was developed, and negative charge density gradually increased until the pH reached 8 (−33.8 mV). The positive charge developed on the amine-functionalized PS/P(MMA-AAm-EGDMA) composite polymer particles is obviously much higher than that on the reference PS/P(MMA-AAm-EGDMA) composite particles. The negative charge developed on the amine-functionalized PS/P(MMA-AAm-EGDMA) composite polymer particles was also higher than that of the reference PS/P(MMA-AAm-EGDMA) composite particles. A portion of the amide and esteric groups present on the surface of composite particles were converted into $-COO^-K^+$ groups by basic hydrolysis during the Hoffman degradation reaction.[48−50]

Figure 7a shows the N_2 adsorption−desorption isotherms of reference PS/P(MMA-AAm-EGDMA) and aminated PS/P(MMA-AAm-EGDMA) composites, which were used to assess their surface area. The observable shapes for both the isotherms of reference and aminated composites are of type-II and type-IV, which render the IUPAC classification of materials. These two composites are mesoporous in nature.[57−59] Unhindered monolayered arrangement or multilayer adsorption is characteristic of the type-II isotherm, whereas a conventional hysteresis loop isotherm is indicated by type-IV. These results are due to the occurrence of capillary condensation in mesopores and limited uptake to the coverage of a wide range of high relative pressure (P/P_0). The surface area of aminated PS/P(MMA-AAm-EGDMA) composites slightly increased (1.79 m^2/g) compared to that of the reference composite (1.61 m^2/g). An increase in the pore volume of the aminated composite was also observed.[60] The values of pore volumes were found to be 0.41 and 0.37 cm^3/g, respectively, while the pore diameter of aminated composites was 35% decreased. The changes in surface area, pore volume, and pore diameter indicate successive surface modification with the copolymer and amine functionalization, and relatively higher values can promote molecular or simple ionic densification in the surface mesopores during the adsorption process. The Barrett−Joyner−Halenda (BJH) method was used to determine the distribution of pore size, pore volume, and pore diameter of the composites. The BJH pore size distribution curves of both composites are shown in Figure 7b. The pore size distribution values were within the range of mesoporous materials (2−50 nm). The pore distribution of the aminated composite was narrow (red curve), which was confirmed by two closer bimodal apexes. The average pore size (4.8 nm) of the aminated composite slightly increased compared to the reference composite. The increase in pore diameter plausibly resulted from the increase in surface heterogeneity followed by decoration with the amine-functionalized copolymer, as indicated by the SEM image (Figure 2c).

Figure 8a shows the magnitude of adsorption of the anionic surfactant SDS at pH 4 and 10 on reference PS/P(MMA-

https://doi.org/10.1021/acsomega.3c02976
ACS Omega 2023, 8, 44523−44536

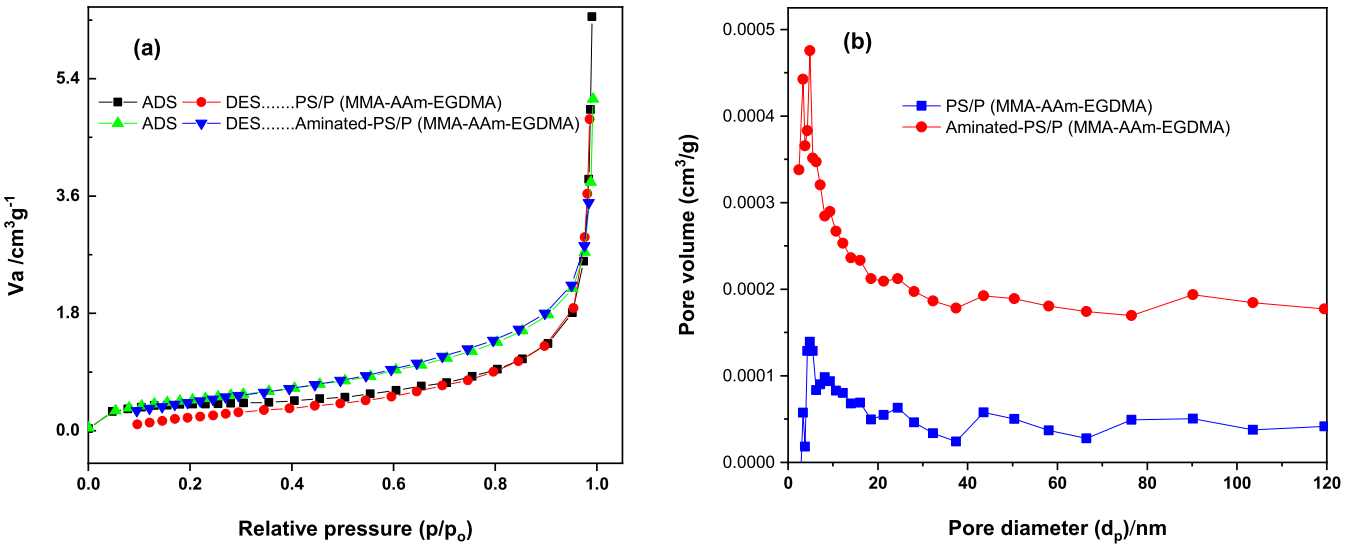

Figure 7. BET N_2 adsorption−desorption isotherms (a) and BJH pore size distributions (b) of reference PS/P(MMA-AAm-EGDMA) and aminated PS/P(MMA-AAm-EGDMA) composite polymer particles.

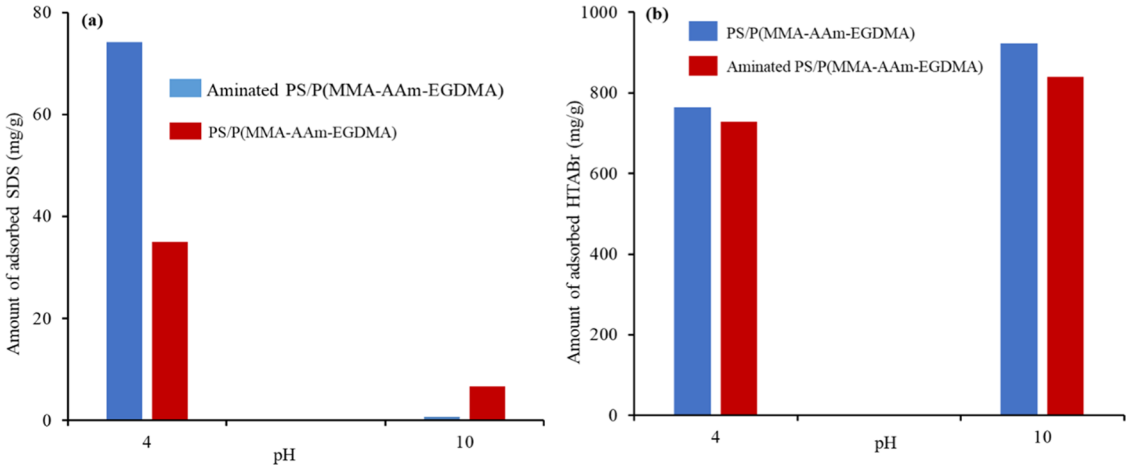

Figure 8. pH-dependent variation of the amount of adsorption for SDS (a) and HTABr (b) by amine-functionalized PS/P(MMA-AAm-EGDMA) and reference PS/P(MMA-AAm-EGDMA) composite polymer particles measured at 25 °C.

AAm-EGDMA) and amine-functionalized PS/P(MMA-AAm-EGDMA) composite polymer particles. The amount of the adsorbed anionic surfactant SDS on amine-functionalized PS/P(MMA-AAm-EGDMA) composite polymer particles was higher (74.14 mg/g) than that on reference PS/P(MMA-AAm-EGDMA) composite polymer particles (34.92 mg/g) at pH 4. This is due to electrostatic attraction between the negatively charged SDS emulsifier and positively charged protonated amine groups present on amine-functionalized PS/P(MMA-AAm-EGDMA) composite particles. On the other hand, at pH 10, the amount of surface adsorption of SDS on amine-functionalized PS/P(MMA-AAm-EGDMA) composite polymer particles is lower (0.64 mg/g) than that on reference PS/P(MMA-AAm-EGDMA) composite particles (6.65 mg/g). These variations were because of the increased repulsion between the negatively charged SDS emulsifier and negatively charged amine-functionalized PS/P(MMA-AAm-EGDMA) composite particles (−33.8 mV). Figure 6b shows the magnitude of adsorption of the cationic surfactant HTABr at two pHs of 4 and 10 on the surface of amine-functionalized and reference composite polymer particles. For both composite particles, the amount of adsorption of the cationic surfactant HTABr at pH 4 was lower than that at pH 10. The amount of the adsorbed cationic surfactant HTABr on amine-functionalized PS/P(MMA-AAm-EGDMA) composite polymer particles was 764.15 mg/g, which was lower than that on reference PS/P(MMA-AAm-EGDMA) composite polymer particles (839.62 mg/g) at pH 4.[51] This decrease in adsorption was due to the electrostatic repulsion between the cationic surfactant HTABr and positively charged protonated amine groups present on the surface of amine-functionalized PS/P(MMA-AAm-EGDMA) composite particles. On the other hand, at pH 10, the amount of adsorption of the cationic surfactant HTABr on the surface of amine-functionalized PS/P(MMA-AAm-EGDMA) composite polymer particles was higher (922.17 mg/g) than that on reference PS/P(MMA-AAm-EGDMA) composite particles (727.45 mg/g). This is because the attraction between the cationic surfactant and negatively charged amine-functionalized PS/P(MMA-AAm-EGDMA) composite particles (−33.8 mV) was higher than the corresponding attraction occurring in the case of reference PS/P(MMA-AAm-EGDMA) composite particles (−8.75 mV).

https://doi.org/10.1021/acsomega.3c02976
ACS Omega 2023, 8, 44523−44536

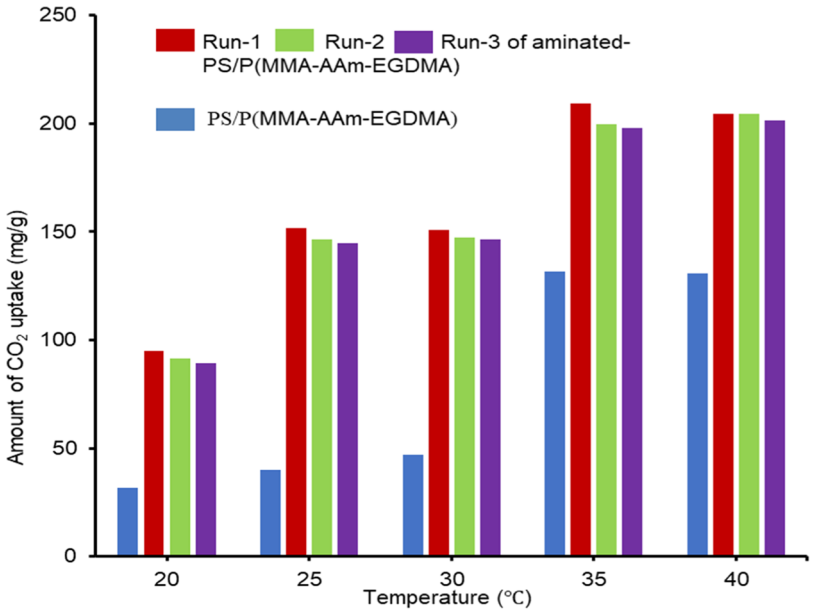

Figure 9. Temperature-dependent CO_2 capturing efficiencies and recycling−reusing of amine-functionalized PS/P(MMA-AAm-EGDMA) composite polymer particles via an aqueous medium.

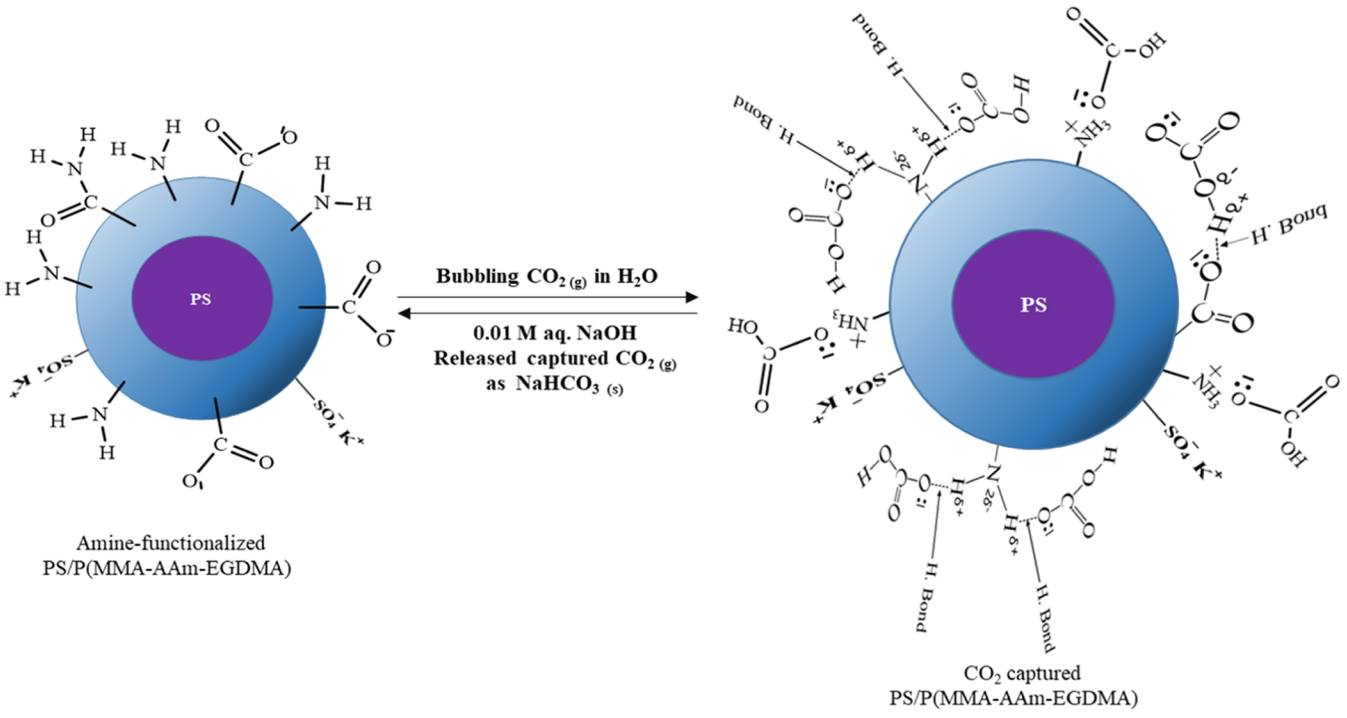

Figure 10. Proposed mechanism of CO_2 capture by amine-functionalized PS/P(MMA-AAm-EGDMA) composite polymer particles via aqueous medium.

Figure 9 exhibits the CO_2-capturing efficiency of amine-functionalized PS/P(MMA-AAm-EGDMA) and reference PS/P(MMA-AAm-EGDMA) composite polymer particles at different temperatures. In Run 1, the amount of capturing CO_2 increased from 136 to 209 mg/g up to the temperature range of 20−35 °C for amine-functionalized composite particles, and then it almost leveled off at 40 °C. In contrast, reference composite particles captured a relatively smaller amount (40−130 mg/g) of CO_2 than aminated composite particles. A sharp change in capturing CO_2 for each composite particle was found in the range of 30−35 °C. It is likely that the increase in thermal vibrations enhanced the mobility of the particles/ions present in the liquid medium.[49] As a result of increased mobility, the particles were dispersed completely in the dispersion medium at higher temperatures, and this effect was dominant in the 30−35 °C temperature range. As a result, the amine groups present on the surface of functionalized particles became fully free from each other, which were activated by carbonic acid via protonation to form $-NH_3^+$. Formed $-NH_3^+$ ions were easily combined via electrostatic attractions with HCO_3^- (Figure 9), which resulted in increased efficiency for capturing CO_2 by amine-functionalized compo-

https://doi.org/10.1021/acsomega.3c02976
ACS Omega 2023, 8, 44523−44536

site polymer particles. In addition, CO_2 gas molecules were also captured by hydrogen bonding through amine and carboxylate moieties of aminated composite polymer particles. On the other hand, reference composite participles also showed quite fair amounts of CO_2 adsorption, although the particles did not contain any amine functionality. It is to be mentioned that the free escaping tendency of CO_2 with increasing temperature might have a great contribution to the reduction of CO_2 capturing on both reference and amine-functionalized composite particles. For recycling and reusing of the aminated particles used in Run 1, the gas-captured adsorbent was treated with aqueous 0.01 M NaOH to recover the aminated composite via centrifugal washing. The recovered aminated composite showed almost similar CO_2 capturing efficiency for additional Runs 2 and 3 under identical conditions. However, a slight decreasing trend in capturing CO_2 was noticed herein due to the inactivation of active adsorption sites via alkali treatment and further washing and drying of the aminated composite polymer particles.

A plausible mechanism for capturing CO_2 by aminated PS/P(MMA-AAm-EGDMA) composite polymer particles is shown in Figure 10. The basic principle of capturing CO_2 in this research is to convert the gaseous CO_2 into its ionic forms, such as protons and bicarbonate ions (HCO_3^-), by using a highly accessible aqueous medium. This ionic conversion is feasible due to the affinity of CO_2 to water. Simply, CO_2 molecules dissolve in water via the formation of H_2CO_3, which readily dissociates in aqueous medium to form protons and bicarbonate ions. These protons and HCO_3^- ions establish an equilibrium with undissociated H_2CO_3. All of these reactions are as follows.

$$H_2O + CO_2(g) \rightarrow H_2CO_3(aq)$$

$$H_2CO_3 \rightleftarrows H^+ + HCO_3^-$$

The generated ionic species, such as protons, are easily consumed by surface amine moieties of the composite particles to form cationic $-NH_3^+$ structures, which are highly prone to attract negatively charged HCO_3^- ions. Besides these amine moieties, the functionalized composite also contained some other groups, like unreacted ester, amide, sulfate, and carboxylate, which also contributed to capturing CO_2 via formation of hydrogen bonding with both the undissociated and dissociated forms of H_2CO_3. These two major factors, such as electrostatic attractions and hydrogen bonding capability of amine-functionalized composite polymer particles, contributed to a high amount of capturing CO_2.

A comparative performance of different adsorbents used for CO_2 adsorption available in the literature is given in Table 2. Most of the materials mentioned in the table have been applied in the packed column, and CO_2 was passed through the bed.[56,62−66] However, in our case, the materials were used directly in an aqueous medium, and CO_2 was bubbled through the medium for interaction. Our method is easy for industrial application and does not require any sophisticated extra device or technology. The interesting finding from the comparison is that our materials can remove a higher amount (4.76 mmol/g) of CO_2 from the gas stream.

Table 2. CO_2 Capture Capacities of Different Adsorbents

different adsorbents	maximum CO_2 adsorption (mmol/g)	references
polymers-loaded mesoporous metal−organic framework PCN-777	1.13	56
polycyclic aromatic hydrocarbon-based microporous organic polymers	3.36	61
PEI-impregnated silica CNT hybrid microtubes	1.92	62
N-doped polyurethane foam-based porous carbons	4.33	63
graphene	3.13	64
PET/dolomite	0.215	65
aminopropyl/PEI	1.39	66
aminated PS/P(MMA-AAm-EGDMA) composite polymer particles	4.76	this work

CONCLUSIONS

In this study, amine-functionalized PS/P(MMA-AAm-EGDMA) composite polymer particles were synthesized by the surface modification of PS seed particles via copolymerization, followed by the Hofmann degradation reaction. The synthesized composite particles have mesopores, pore diameter, moderate specific surface area, spherical shape, and zwitterionic properties. The particles effectively showed a pH-responsive adsorption property for both anionic and cationic surfactants. This pH-dependent surface-active property of the particles assisted in the capture of CO_2 bubbling through an aqueous medium. In temperature-variable measurements, a maximum CO_2 adsorption of 209 mg/g was achieved at 35 °C by the aminated composite particles. The synthesized composite particles showed almost the same CO_2 adsorption efficiency up to the third cycle. During CO_2 adsorption, no remarkable environment-threatening byproduct except $NaHCO_3$ was produced. Herein, a simple separation technique is followed, which is inexpensive and easily accessible. The process was carried out under normal atmospheric pressure. Despite significant technical and structural challenges throughout the investigation, the obtained results are encouraging enough to motivate further research with precise design. Using our amine-functionalized composite polymer particles, other acidic gases, contaminated water with acidic dyes, and various mineral acids can also be removed.

ASSOCIATED CONTENT

Supporting Information

The Supporting Information is available free of charge at https://pubs.acs.org/doi/10.1021/acsomega.3c02976.

Conversion of styrene into polystyrene; digital images of the conversion of PS/P(MMA-AAm-EGMA) into aminated PS/P(MMA-AAm-EGMA) composite particles; calibration curves of emulsifiers; SEM-EDX elemental mapping of PS/P(MMA-AAm-EGDMA) composite polymer particles; and pH change curves due to passing of CO_2 through aqueous dispersions (PDF)

AUTHOR INFORMATION

Corresponding Authors

Md. Abdur Rahman − *Research Laboratory of Polymer Colloids and Nanomaterials, Department of Chemistry, Faculty of Science, Rajshahi University, Rajshahi 6205, Bangladesh;* orcid.org/0000-0002-3855-8160; Email: arahman@ru.ac.bd

Md. Ashraful Alam − *Research Laboratory of Polymer Colloids and Nanomaterials, Department of Chemistry,*

https://doi.org/10.1021/acsomega.3c02976
ACS Omega 2023, 8, 44523−44536

Faculty of Science, Rajshahi University, Rajshahi 6205, Bangladesh; Email: aashraful41@ru.ac.bd

Authors

M. Asheq Mahamud − *Research Laboratory of Polymer Colloids and Nanomaterials, Department of Chemistry, Faculty of Science, Rajshahi University, Rajshahi 6205, Bangladesh*

A. S. M. Maruf Galib − *Research Laboratory of Polymer Colloids and Nanomaterials, Department of Chemistry, Faculty of Science, Rajshahi University, Rajshahi 6205, Bangladesh*

Md. Muhyminul Islam − *Research Laboratory of Polymer Colloids and Nanomaterials, Department of Chemistry, Faculty of Science, Rajshahi University, Rajshahi 6205, Bangladesh*

Md. Mahiuddin − *Khulna University, Khulna 9208, Bangladesh*; orcid.org/0000-0002-1195-9159

Md. Mahbubor Rahman − *Research Laboratory of Polymer Colloids and Nanomaterials, Department of Chemistry, Faculty of Science, Rajshahi University, Rajshahi 6205, Bangladesh*; orcid.org/0000-0002-6763-525X

Md. Shahidul Islam − *Research Laboratory of Polymer Colloids and Nanomaterials, Department of Chemistry, Faculty of Science, Rajshahi University, Rajshahi 6205, Bangladesh*

Hasan Ahmad − *Research Laboratory of Polymer Colloids and Nanomaterials, Department of Chemistry, Faculty of Science, Rajshahi University, Rajshahi 6205, Bangladesh*; orcid.org/0000-0003-1499-167X

Complete contact information is available at: https://pubs.acs.org/10.1021/acsomega.3c02976

Notes

The authors declare no competing financial interest.

■ ACKNOWLEDGMENTS

The authors are thankful to Professor Dr. Bungo Ochiai, Department of Chemistry and Chemical Engineering, Graduate School of Science and Engineering, Yamagata University, Japan, for analyzing samples. The project director is grateful to the Central Science Laboratory, Rajshahi University. The authors are also grateful to the Faculty of Science, Rajshahi University, for the financial support.

■ REFERENCES

(1) Yoro, K. O.; Daramola, M. O. *CO_2 Emission Sources, Greenhouse Gases, and the Global Warming Effect*; Elsevier Inc., 2020; pp 3−28.

(2) https://www.statista.com/statistics/1091926/atmospheric-concentration-of-co2-historic/.

(3) Markewitz, P.; Kuckshinrichs, W.; Leitner, W.; Linssen, J.; Zapp, P.; Bongartz, R.; Schreiber, A.; Müller, T. E. Worldwide innovations in the development of carbon capture technologies and the utilization of CO_2. *Energy Environ. Sci.* **2012**, *5*, 7281−7305.

(4) Yu, C. H.; Huang, C. H.; Tan, C. S. A review of CO_2 capture by absorption and adsorption. *Aerosol Air Qual. Res.* **2012**, *12*, 745−769.

(5) Samanta, A.; Zhao, A.; Shimizu, G. K. H.; Sarkar, P.; Gupta, R. Post-Combustion CO_2 Capture Using Solid Sorbents. A Review. *Ind. Eng. Chem. Res.* **2012**, *51*, 1438−1463.

(6) Choi, S.; Drese, J. H.; Jones, C. W. Adsorbent Materials for Carbon Dioxide Capture from Large Anthropogenic Point Sources. *ChemSusChem* **2009**, *2*, 796−854.

(7) Songolzadeh, M.; Ravanchi, M. T.; Soleimani, M. Carbon Dioxide Capture and Storage: A General Review on Adsorbents. *World Acad. Sci. Eng. Technol.* **2012**, *70*, 225−232.

(8) D'Alessandro, D.; Smit, B.; Long, J. R. Carbon Dioxide Capture: Prospects for New Materials. *Angew. Chem., Int. Ed.* **2010**, *49*, 6058−6082.

(9) Song, C. Global challenges and strategies for control, conversion and utilization of CO_2 for sustainable development involving energy, catalysis, adsorption and chemical processing. *Catal. Today* **2006**, *115*, 2−32.

(10) Merkel, T. C.; Lin, H.; Wei, X.; Baker, R. Power plant post-combustion carbon dioxide capture: An opportunity for membranes. *J. Membr. Sci.* **2010**, *359*, 126−139.

(11) Thompson, R. L.; Thompson, T.; Culp, J.; Tiwari, S. P.; Basha, O. M.; Shi, W.; Damodaran, K.; Resnik, K.; Siefert, N. S.; Hopkinson, D. P. Effect of Molecular Structure on the CO_2 Separation Properties of Hydrophobic Solvents Consisting of Grafted Poly Ethylene Glycol and Poly Dimethyl Siloxane Units. *Energy Fuels* **2019**, *33*, 4432−4441, DOI: 10.1021/acs.energyfuels.9b00500.

(12) Park, J.; Park, J. R.; Choe, J. H.; Kim, S.; Kang, M.; Kang, D. W.; Kim, J. W.; Jeong, Y. W.; Hong, C. S. Metal−Organic Framework Adsorbent for Practical Capture of Trace Carbon Dioxide. *ACS Appl. Mater. Interfaces* **2020**, *12*, 50534−50540, DOI: 10.1021/acsami.0c16224.

(13) Park, J.; Chae, Y. S.; Kang, D. W.; Kang, M.; Choe, J. H.; Kim, S.; Kim, J. Y.; Jeong, Y. W.; Hong, C. S. Shaping of a Metal−Organic Framework−Polymer Composite and Its CO_2 Adsorption Performances from Humid Indoor Air. *ACS Appl. Mater. Interfaces* **2021**, *13*, 25421−25427.

(14) Sattari, A.; Ramazani, A.; Aghahosseinim, H.; Aroua, M. K. The application of polymer containing materials in CO_2 capturing via absorption and adsorption methods. *J. CO_2 Util.* **2021**, *48*, No. 101526.

(15) Xu, T.; Wu, Q.; Chen, S.; Denga, M. Preparation of polypropylene based hyperbranched absorbent fibers and the study of their adsorption of CO_2. *RSC Adv.* **2015**, *5*, 32902−32908.

(16) Yaumi, A. L.; Abu Bakar, M. Z.; Hameed, B. H. Recent advances in functionalized composite solid materials for carbon dioxide capture. *Energy* **2017**, *124*, 461−480.

(17) Wang, W.; Wang, X.; Song, C.; Wei, X.; Ding, J.; Xiao, J. Sulfuric Acid Modified Bentonite as the Support of Tetraethylenepentamine for CO_2 Capture. *Energy Fuels* **2013**, *27*, 1538−1546.

(18) Fauth, D. J.; Gray, M. L.; Pennline, H. W.; et al. Investigation of Porous Silica Supported Mixed-Amine Sorbents for Post-Combustion CO_2 Capture. *Energy Fuels* **2012**, *26*, 2483−2496.

(19) Zhao, L.; Bacsik, Z.; Hedin, N.; Wei, W.; Sun, Y.; Antonietti, M.; Magdalena Titirici, M. Carbon Dioxide Capture on Amine-Rich Carbonaceous Materials Derived from Glucose. *ChemSusChem* **2010**, *3*, 840−845.

(20) Alesi, W. R., Jr.; Kitchin, J. R. Evaluation of a Primary Amine-Functionalized Ion-Exchange Resin for CO_2 Capture. *Ind. Eng. Chem. Res.* **2012**, *51*, 6907−6915.

(21) Ghosh, A. K.; Dwivedi, M. Advantages and Applications of Polymeric Composites. In *Processability of Polymeric Composites*; Springer: New Delhi, 2020 DOI: 10.1007/978-81-322-3933-8_2.

(22) Drese, B. J. H.; Choi, S.; Lively, R. P.; Koros, W. J.; Fauth, D. J.; Gray, M. L.; Jones, C. W. Synthesis−Structure−Property Relationships for Hyperbranched Aminosilica CO_2 Adsorbents. *Adv. Funct. Mater.* **2009**, *19*, 3821−3832.

(23) Qi, G.; Wang, Y.; Estevez, L.; Duan, X.; Anako, N.; Park, A. A.; Li, W.; Jonesc, C. W.; Giannelis, E. P. High efficiency nanocomposite sorbents for CO_2 capture based on amine-functionalized mesoporous capsules. *Energy Environ. Sci.* **2011**, *4*, 444−452.

(24) Dao, D. S.; Yamada, H.; Yogo, K. Large-Pore Mesostructured Silica Impregnated with Blended Amines for CO_2 Capture. *Ind. Eng. Chem. Res.* **2013**, *52*, 13810−13817.

(25) Fujiki, J.; Yogo, K. Polyethyleneimine-functionalized Biomass-derived Adsorbent Beads for Carbon Dioxide Capture under Ambient Conditions. *Chem. Lett.* **2013**, *42*, 1484−1486.

(26) Fujiki, J.; Yogo, K. Carbon Dioxide Adsorption onto Polyethylenimine-Functionalized Porous Chitosan Beads. *Energy Fuels* **2014**, *28*, 6467−6474.
(27) Gao, H.; Li, Q.; Ren, S. Recent advances on CO_2 capture by porous organic polymers. *Curr. Opin. Green Sustainable Chem.* **2019**, *16*, 33−38.
(28) Chang, D.; Yu, M.; Zhang, C.; Zhao, Y.; Kong, R.; Xie, F.; Jiang, J. X. Indolo[3,2-b] carbazole-containing hypercrosslinked microporous polymer networks for gas storage and separation. *Microporous Mesoporous Mater.* **2016**, *228*, 231−236.
(29) Gao, H.; Ding, L.; Bai, H.; Liu, A.; Lib, S.; Li, L. Pitch-based hyper-cross-linked polymers with high performance for gas adsorption. *J. Mater. Chem. A* **2016**, *4*, 16490.
(30) Tian, Y.; Qi Xu, S.; Qian, C.; Fu Pang, Z.; Jiang, G. F.; Zhao, X. Two-dimensional dual-pore covalent organic frameworks obtained from the combination of two D2h symmetrical building blocks. *Chem. Commun.* **2016**, *52*, 11704.
(31) Li, J. J. *Name Reactions − A Collection of Detailed Reactions Mechanism*; Springer-Verlag GmbH: Berlin, 2002.
(32) Morel, F. M.; Hering, J. G. *Principles and Applications of Aquatic Chemistry*; John Wiley & Sons, 1993.
(33) Ahmad, H.; Hossain, M. E.; Rahman, M. A.; Rahman, M. M.; Miah, M. A. J.; Tauer, K. Carboxyl functionalized poly-(methylmethacrylate-acrylic acid-ethylene glycol dimethacrylate) copolymer particles and their amination with amine-nucleophiles. *e-Polymers* **2008**, *8*, No. 1109, DOI: 10.1515/epoly.2008.8.1.1109.
(34) Rahman, M. A.; Karim, M. R.; Miah, M. A. J.; Ahmad, H.; Yamashita, T. Encapsulation of submicron-sized silica particles by stimuli-responsive copolymer shell layer. *Macromol. Res.* **2010**, *18*, 247−253.
(35) Shathi, T. S.; Rahman, M. A.; Nasiruddin, M.; Alim Al-Bari, M. A.; Pande, S.; Komeda, T.; Ul-Hamid, A.; Ahmad, H.; Ahmad, H.; Karim, M. R. Synthesis and functionalization of zinc phosphate@ polyglycidyl methacrylate composites for antimicrobial drug immobilization and controlled release: an in vitro study. *New J. Chem.* **2023**, *47*, 14534−14550.
(36) Rahman, M. A.; Miah, M. A. J.; Ahmad, H. Controlling surface hydrophilicity of silica particles via seeded copolymerization and their characterization. *J. Polym. Mater.* **2012**, *29*, 217−227.
(37) Rahman, M. A.; Miah, M. A. J.; Minami, H.; Ahmad, H. Preparation of magnetically doped multilayered functional silica particles via surface modification with organic polymer. *Polym. Adv. Technol.* **2013**, *24*, 174−180.
(38) Jannat, N. E.; Alam, M. A.; Rahman, M. A.; Rahman, M. M.; Hossain, M. K.; Hossain, S.; Minami, H.; Ahmad, H. Carboxylic acid modified pH-responsive composite polymer particles. *J. Polym. Eng.* **2019**, *39*, 671−678.
(39) Sharma, Y. R. *Elementary Organic Spectroscopy*, 4 th ed.; S. Chand Publishing, 2007.
(40) Pavia, D. L.; Lampman, G. M.; Kriz, G. S. *Introduction to Spectroscopy*, 6th ed.; Thomson Learning, 2013.
(41) Liang, C. Y.; Krimm, S.; Randall, H. M. Infrared spectra of high polymers. VI. Polystyrene. *J. Polym. Sci.* **1958**, *XXVII*, 241−254, DOI: 10.1002/pol.1958.1202711520.
(42) https://en.wikipedia.org/wiki/Infrared-spectroscopy.
(43) http://www.chem.ucla.edu/~harding/IGOC/F/fingerprint-region.htmlwww.chem.ucla.edu/~harding/IGOC/F/fingerprint-region.html.
(44) Rosemal, M. H.; Haris, M.; Kathiresan, S.; Mohan, S.. Scholars Research Library 2010, *2*, 316−323.
(45) Yang, K.; Chen, J.; Fu, Q.; Dun, X.; Yao, C. Preparation of novel amphoteric polyacrylamide and its synergistic retention with cationic polymers. *e-Polymers* **2020**, *20*, 162−170.
(46) Yamaura, M.; Camilo, R. L.; Sampaio, L. C.; Macedo, M. A.; Nakamura, M.; Toma, H. E. Preparation and characterization of (3-aminopropyl)triethoxysilane-coated magnetite nanoparticles. *J. Magn. Magn. Mater.* **2004**, *279* (2−3), 210−217, DOI: 10.1016/j.jmmm.2004.01.094.
(47) White, L. D.; Tripp, C. P. Reaction of (3-Aminopropyl)-dimethylethoxysilane with Amine Catalysts on Silica Surfaces. *J. Colloid Interface Sci.* **2000**, *232* (2), 400−407, DOI: 10.1006/jcis.2000.7224.
(48) Smets, G.; De Loecker, W. Alkaline hydrolysis of methacrylic acid−ester copolymers. *J. Polym. Sci.* **1959**, *XLI*, 375−380.
(49) Martin, R. B. Acid-catalyzed ester hydrolysis. *J. Am. Chem. Soc.* **1967**, *89* (10), 2501−2502.
(50) Zahn, D. Theoritical study of the mechanism of acid-catalyzed amide hydrolysis in aqueous solution. *J. Phys. Chem. A* **2003**, *107*, 12303−12306.
(51) Tanjim, M.; Rahman, M. A.; Rahman, M. M.; Minami, H.; Hoque, S. M.; Sharafat, M. K.; Gafur, M. A.; Ahmad, H. Mesoporous magnetic silica particles modified with stimuli-responsive P(NIPAM-DMA) valve for controlled loading and release of biologically active molecules. *Soft Matter* **2018**, *14*, 5469−5479.
(52) Debnath, M. K.; Rahman, M. A.; Minami, H.; Rahman, M. M.; Alam, M. A.; Sharafat, M. K.; Hossain, M. K.; Ahmad, H. Single step modification of micrometer-sized polystyrene particles by electromagnetic polyaniline and sorption of chromium(VI) metal ions from water. *J. Appl. Polym. Sci.* **2019**, *136*, 47524.
(53) Bristy, S. S.; Rahman, M. A.; Tauer, K.; Minami, H.; Ahmad, H. Preparation and characterization of magnetic γ-Al_2O_3 ceramic nanocomposite particles with variable Fe_3O_4 content and modification with epoxide functional polymer. *Ceram. Int.* **2018**, *44*, 3951−3959.
(54) Tagliavini, M.; Weidler, P. G.; Njel, C.; Pohl, J.; Richter, D.; Böhringer, B.; Schäfer, A. I. Polymer-based spherical activated carbon−ultrafiltration (UF-PBSAC) for the adsorption of steroid hormones from water: material characteristics and process configuration. *Water Res.* **2020**, *185*, No. 116249.
(55) Bandara, P. C.; Peña-Bahamonde, J.; Rodrigues, D. F. Redox mechanisms of conversion of Cr(VI) to Cr(III) by graphene oxide-polymer composite. *Sci. Rep.* **2020**, *10*, No. 9237.
(56) Smith, M.; Scudiero, L.; Espinal, J.; McEwen, J.-S.; Garcia-Perez, M. Improving the deconvolution and interpretation of XPS spectra from chars by ab initio calculations. *Carbon* **2016**, *110*, 155−171.
(57) Park, J. M.; Jhung, S. H. CO_2 adsorption at low pressure over polymers-loaded mesoporous metal organic framework PCN-777: effect of basic site and porosity on adsorption. *J. CO_2 Util.* **2020**, *42*, No. 101332.
(58) Ryu, Z.; Zheng, J.; Wang, M.; Zhang, B. Characterization of pore size distributions on carbonaceous adsorbents by DFT. *Carbon* **1999**, *37*, 1257−1264.
(59) Li, Y.; Li, Z.; Shen, P. K. Simultaneous formation of ultrahigh surface area and three-dimensional hierarchical porous graphenelike networks for fast and highly stable supercapacitors. *Adv. Mater.* **2013**, *25*, 2474−2480.
(60) Sing, K. S. W.; Everett, D. H.; Haul, R. A. W.; Moscou, L.; Pierotti, R. A.; Rouquérol, J.; Siemieniewska, T. Reporting physisorption data for gas/solid systems with special reference to the determination of surface area and porosity. *Pure Appl. Chem.* **1985**, *57*, 603−619.
(61) Hou, S.; Wang, S.; Long, X.; Tan, B. Knitting polycyclic aromatic hydrocarbon-based microporous organic polymers for efficient CO_2 capture. *RSC Adv.* **2018**, *8*, 10347−10354.
(62) Keller, L.; Ohs, B.; Abduly, L.; Wessling, M. Carbon nanotube silica composite hollow fibers impregnated with polyethylenimine for CO_2 capture. *Chem. Eng. J.* **2018**, *18*, 32334−32339, DOI: 10.1016/j.cej.2018.11.100.
(63) Ge, C.; Song, J.; Qin, Z.; Wang, J.; Fan, W. Polyurethane foam-based ultra-microporous carbons for CO_2 capture. *ACS Appl. Mater. Interfaces* **2016**, *8*, 18849.
(64) Tian, Y.; Lin, Y.; Hagio, T.; Hu, Y. H. Surface-microporous graphene for CO_2 adsorption. *Catal. Today* **2020**, *356*, 514−518.
(65) Przepiórski, J.; Czyżewski, A.; Pietrzak, R.; Morawski, A. W. MgO/CaO-loaded activated carbon for carbon dioxide capture: practical aspects of use. *Ind. Eng. Chem. Res.* **2013**, *52*, 6669−6677.

(66) Sanz, R.; Calleja, G.; Arencibia, A.; Sanz-Pérez, E. S. CO_2 capture with pore-expanded MCM-41 silica modified with amino groups by double functionalization. *Microporous Mesoporous Mater.* **2014**, *209*, 165−171, DOI: 10.1016/j.micromeso.2014.10.045.

https://doi.org/10.1021/acsomega.3c02976
ACS Omega 2023, 8, 44523−44536